Smurf1 Modulates Smad Signaling Pathway in Fibrotic Cataract Formation

Fanying Jiang, Yuanfan Yang, Yan Ni, Yingyan Qin, Fa Yuan, Rong Ju, and Mingxing Wu

State Key Laboratory of Ophthalmology, Zhongshan Ophthalmic Center, Sun Yat-Sen University, Guangdong Provincial Key Laboratory of Ophthalmology and Visual Science, Guangzhou, China

Correspondence: Mingxing Wu, State Key Laboratory of Ophthalmology, Zhongshan Ophthalmic Center, Sun Yat-Sen University, Guangdong Provincial Key Laboratory of Ophthalmology and Visual Science, No. 7 Jinsui Road, Guangzhou 510060, China; wumingx@mail.sysu.edu.cn.
Rong Ju, State Key Laboratory of Ophthalmology, Zhongshan Ophthalmic Center, Sun Yat-Sen University, Guangdong Provincial Key Laboratory of Ophthalmology and Visual Science, No. 7 Jinsui Road, Guangzhou 510060, China; jurong@mail.sysu.edu.cn.

Received: September 11, 2023
Accepted: January 25, 2024
Published: February 7, 2024

Citation: Jiang F, Yang Y, Ni Y, et al. Smurf1 modulates smad signaling pathway in fibrotic cataract formation. *Invest Ophthalmol Vis Sci.* 2024;65(2):18. https://doi.org/10.1167/iovs.65.2.18

Purpose. TGF-β/BMP signaling pathway plays a significant role in fibrotic cataract. Smurf1, a ubiquitin protein ligase, regulates the TGF-β/BMP signaling pathway through the ubiquitin-proteasome system (UPS). This study aims to investigate the role of Smurf1 in the progression of fibrotic cataract and its underlying mechanism.

Methods. We used a mouse model of injury-induced anterior subcapsular cataract (ASC) and administered the Smurf1 inhibitor A01 for in vivo investigations. RNA sequencing was performed to examine global gene expression changes. Protein levels were assessed by Simple Western analysis. The volume of subcapsular opacity was determined using whole-mount immunofluorescence of lens anterior capsules. Lentivirus was utilized to establish cell lines with Smurf1 knockdown or overexpression in SRA01/04. Lens epithelial cell (LEC) proliferation was evaluated by CCK8 and EdU assays. Cell cycle profile was determined by flow cytometry. LEC migration was measured using Transwell and wound healing assays.

Results. The mRNA levels of genes associated with cell proliferation, migration, epithelial-mesenchymal transition (EMT), TGF-β/BMP pathway, and UPS were upregulated in mouse ASC model. Smurf1 mRNA and protein levels were upregulated in lens capsules of patients and mice with ASC. Anterior chamber injection of A01 inhibited ASC formation and EMT. In vitro, Smurf1 knockdown reduced proliferation, migration and TGF-β_2-induced EMT of LECs, concomitant with the upregulation of Smad1, Smad5, and pSmad1/5. Conversely, overexpression of Smurf1 showed opposite phenotypes.

Conclusions. Smurf1 regulates fibrotic cataract progression by influencing LEC proliferation, migration, and EMT through the modulation of the Smad signaling pathway, offering a novel target for the fibrotic cataract treatment.

Keywords: Smurf1, fibrotic cataract, Smad, lens epithelial cell (LEC)

Fibrotic cataract encompasses posterior capsular opacification (PCO) and anterior subcapsular cataract (ASC). PCO is a common delayed postoperative complication that impairs visual quality despite advanced surgical techniques, instrumentation, and intraocular lens materials.[1–3] Surgical trauma stimulates residual lens epithelial cells (LECs), triggering a wound-healing response distinguished by migration, proliferation, and EMT, culminating in PCO development.[4,5] ASC, on the other hand, can be caused by surgical trauma,[6,7] ultraviolet radiation exposure,[8] other ocular diseases like retinitis pigmentosa,[9,10] and systemic diseases such as atopic dermatitis.[11,12] PCO and ASC share a common pathological mechanism involving abnormal proliferation, migration, and EMT of LECs, leading to subcapsular fibrotic opacification formation.[13]

Transforming growth factor beta (TGF-β) is a widely recognized cytokine with an established role in promoting the migration and EMT of LECs,[14–16] thus considered as a primary inducer for cataract pathogenesis.[17,18] On the other hand, bone morphogenic proteins (BMPs), which are members of the TGF-β superfamily, were found to play an opposite role in these processes.[19,20] Our recent findings showed that LEC proliferation, migration, and EMT were suppressed by BMP-4 and BMP-7 in a mouse ASC model.[16] Upon binding to their respective ligands, the TGF-β/BMP receptors activate receptor-regulated Smad proteins (R-Smads), including Smad2 and Smad3 for TGF-β signaling, and Smad1, Smad5, and Smad8 for BMP signaling. These R-Smads, along with a nuclear Smad called Smad4, form a complex that recruits transcriptional co-regulators to modulate gene transcription downstream of TGF-β/BMP signaling within the nucleus.[21–23] The contrasting effects between TGF-βs and BMPs appear to be executed via the complicated interactions among Smads.[20]

TGF-β/BMP signaling can be regulated by the ubiquitin-proteasome pathway (UPP).[24] Initially reported as an inducer of degradation for BMP pathway-specific R-Smads (Smad1 and Smad5), Smad ubiquitin regulatory factor 1 (Smurf1), also referred to as SMAD Specific E3 Ubiquitin Protein Ligase 1, has been identified.[25] On the other hand, Smad2 and Smad3 are modulated by Smurf2, which has a distinct role from Smurf1.[26–28] Smurf1 was shown to promote the migration, proliferation, as well as invasiveness of gastric cancer cells.[29] Additionally, Smurf1 was found

to enhance the invasiveness of pancreatic cancer, prostate cancer, and glioblastoma.[30–32] Inhibiting Smurf1 ameliorated retinal injury in $NaIO_3$-induced dry age-related macular degeneration mice by modulating EMT and the inflammatory response.[33]

To investigate the role of Smurf1 in fibrotic cataract, this study delves deeper into Smurf1's function in the regulation of the biological behavior of LECs, the progression of fibrotic cataract, and the detailed regulatory impact of Smurf1 on Smads within LECs.

Materials and Methods

Injury-Induced ASC Model in the Mouse

Animal experiments adhered to the guidelines of the Ethics Committee of Zhongshan Ophthalmic Center (Z2022013) and the ARVO Statement for the Use of Animals in Ophthalmic and Vision Research. Adult C57BL/6 mice aged 6 to 8 weeks were utilized to create the injury-induced ASC model, as previously described.[34] Briefly, mice were generally anesthetized with intraperitoneal injection of pentobarbital sodium (50 mg/kg). Compound tropicamide eye drops were used for pupillary dilation, and proparacaine hydrochloride eye drops were applied topically for anesthesia. A small incision was made at the center of the anterior capsule by vertically inserting a 26-gauge hypodermic needle through the cornea. The depth of insertion reached a quarter of the blade's length (approximately 300 µm). Following surgery, 50 µM A01 (SML1404; Sigma-Aldrich, Merck KGaA, Darmstadt, Germany) was injected into the anterior chamber with a Hamilton microsyringe. The consistent depth and angle of needling ensured uniform incision sizes. Tobramycin eye ointment was used postoperatively to prevent infection. The mice were euthanized 7 days after the surgery, and the lens capsules were collected for experiments.

RNA Sequence Analysis

Total RNA was extracted from lens capsules or LECs with the Trizol reagent (RNAiso Plus; Takara Bio Inc., Shiga, Japan), with each group comprising four biological replicates. The quantification of RNA was assessed by Nanodrop 2000 (Thermo Fisher Scientific, Waltham, MA, USA), and the RNA integrity was measured by the Agilent Fragment Analyzer 5400 (Agilent Technologies, Santa Clara, CA, USA). Samples with a total quantity over 400 ng and an RNA Integrity Number exceeding 7 are considered qualified. The sequencing libraries was generated by Illumina (New England Biolabs Inc., Ipswich, MA, USA). The differential expression of genes was analyzed by DESeq2 R package (version 1.20.1) and $|\log2(\text{fold change})| > 0$ and $padj < 0.05$ were used as the criteria for differential gene selection. We used the clusterProfiler R package for Gene Ontology (GO) analysis. RNA sequence data reported in this article have been deposited in the NCBI FEO database under accession number GSE245412.

Quantitative Real-Time PCR

Total RNA of human or mouse lens capsules was extracted using TRIzol reagent (RNAiso Plus, Takara). The reverse transcription was completed with the FastKing RT Kit (KR116; Tiangen Biotech Co., Ltd., Beijing, China). ChamQ SYBR qPCR Master Mix (Q331; Vazyme Biotech Co., Ltd., Nanjing, China) was utilized for quantitative real-time PCR in a QuantStudio 7 Flex (Thermo Fisher Scientific). Primer sequences are provided in Supplementary Table S1.

Simple Western Analysis

RIPA buffer supplemented with protease and phosphatase inhibitors (Roche, Basel, Switzerland) was utilized to lyse lens capsules or LECs. The protein sample concentrations were determined using the BCA-100 Protein Assay Kit (Biocolor Bioscience & Technology Co., Ltd., Shanghai, China). The biotinylated ladder, blocking buffer, and the chemiluminescent substrate provided in the detection module (DM-001 and DM-002, ProteinSimple, Bio-Techne, Minneapolis, MN, USA), along with the denatured protein samples, diluted primary, and secondary antibodies (see Supplementary Tables S2, S3) were loaded into designated wells of a prefilled Wes Separation 12-230 kDa plate provided in the separation module (SM-W004; Bio-Techne). The separation and detection were performed automatically in the capillaries loaded onto the instrument (Wes; Bio-Techne) following the manufacturer's instructions. Data analysis and results presentation were performed using Compass for SW software (version 6.0). Specifically, relative protein expression was quantified by dividing the area of the chemiluminescent peak of the protein of interest by that of the β-actin loading control, with the system automatically determining the high dynamic range (HDR) exposure. The electrophoretograms, generated by the software based on the area of chemiluminescent peaks, were utilized for presenting the results. Standard curves were generated following the manufacturer's instructions to confirm that the final total protein concentration used in this study (1 µg/µL) fell within the linear range, as illustrated in Supplementary Figure S1.

Collections of Human Lens Capsules

The research was in accordance with the approved guidelines of the Ethics Committee of the Zhongshan Ophthalmic Center (Approval No. R016). The anterior capsules of transparent lenses were sourced from cadaveric eyes at the eye bank of the Zhongshan Ophthalmic Center. Additionally, the anterior capsules were collected from patients observed to have ASC both through pre-operative slit lamp examination and intra-operative observation under an operating microscope. All surgical procedures were performed by Dr. Mingxing Wu, and the diameter of the capsule samples averaged approximately 5 mm. Prior to surgery, informed consent was obtained from all participating patients. Detailed information about the donors and patients is provided in Supplementary Tables S4 and S5.

Immunofluorescence

Lens anterior capsules or cell slides were fixed with methanol for 1 hour at room temperature, and subsequently rinsed 3 times with PBS. Blocking and permeabilization were performed using a solution of 5% bovine serum albumin (BSA; BioFroxx, Shanghai, China) diluted in PBS with 0.5% Triton X-100. Following overnight incubation with primary antibodies at 4°C, the tissues and cells were subsequently incubated with an FITC-conjugated antibody and 1 µg/mL

DAPI for 1 hour at room temperature. The primary and secondary antibodies are listed in Supplementary Tables S2 and S3. Images were captured using the ZEISS LSM 980 confocal microscope. The Z-stack mode and the LSCM Image Browser software were used for the 3D reconstruction and volume calculation of the plaque, as previously described.[34] Briefly, the entire plaque was scanned continuously from top to bottom with a 1 µm interval. The opacity exhibited a shape akin to a stack of superimposed pyramidal frustums. Frustum volume between each pair of images was computable using the frustum volume formula: $V_1 = 1/3 \times H \times [S_1 + S_2 + \sqrt{S_1 \times S_2}]$, (V = volume, H = altitude of frustum, 1 µm in our study, S_1 = base area 1, and S_2 = base area 2). Therefore, the volume of a subcapsular plaque equals the aggregate of individual volumes between each pair of images ($V_{total} = V_1 + V_2 + \ldots\ldots + V_n$, V_{total} = volume of subcapsular plaque, V_n = individual volumes between 2 images). Six samples of anterior lens capsules were utilized for statistical analysis in each group.

Cell Culture and Treatment

The human LEC line SRA01/04 was cultured in Dulbecco's Modified Eagle's Medium (DMEM; Gibco, Life Technologies Corporation, Grand Island, NY, USA) supplemented with 10% fetal bovine serum (FBS; Gibco), 100 IU/mL penicillin, and 100 µg/mL streptomycin (Gibco). LECs were treated with 20 ng/mL recombinant human TGF-β_2 (PeproTech, Cranbury, NJ, USA) for the specified duration. Stable cell lines with Smurf1 knockdown and overexpression were constructed using lentivirus. To develop lentivirus, transfection reagent lipofectamine 2000 (Invitrogen, Thermo Fisher Scientific) and viral particles (psPAX2 packaging and pMD2.G envelope plasmids) with shSmurf1, control shRNA, pLVX-SMURF1-HA-Puro, or its mutant plasmid (Dahong Biotechnology Corporation, Guangdong, China) were transfected into HEK293T cells. After 48 hours, the supernatant of the culture medium, which contained lentivirus, was collected, and fresh media were added to the HEK293T cells. The filtered supernatant was transferred to each well of SRA01/04 cells. Positive cells were screened using 2 µg/mL puromycin. The pooled cells were harvested and their knockdown efficiency and overexpression level were confirmed by Western blot. These knockdown and overexpression cell lines were utilized for subsequent experiments and cultured in medium supplemented with 1.5 µg/mL puromycin.

Cell Counting Kit-8 Assay and Proliferation Assay

LEC viability was determined using the CCK-8 (K1018; ApexBio Technology, Houston, TX, USA). LECs were cultured in a 96-well plate with DMEM supplemented with FBS for 24 hours. Subsequently, 100 µL of DMEM containing 10% CCK-8 assay reagent was added to each well, followed by incubation for 2 hours at 37°C. The Infinite M200 Pro NanoQuant was used for the measurement of the optical density (OD) value at 450 nm. Cell proliferation was assessed using an EdU cell proliferation kit (BeyoClickTM EdU Cell Proliferation Kit with Alexa Fluro 594, C0078S; Beyotime, Shanghai, China). LECs seeded in a 12-well plate were incubated with EdU labeling reagent for 2 hours. Following fixation and permeabilization, the click reaction mixture was added to the LECs. Images were captured using a ZEISS LSM 980 confocal microscope.

Flow Cytometry Analysis

The cells were fixed in 75% ethanol overnight at 4°C, after which the cells were washed twice with PBS. Subsequently, 0.5 mL of FxCycle PI/RNase Staining Solution (Life Technologies, Thermo Fisher Scientific) stain was added to each sample and was incubated for 30 minutes at room temperature in the dark. The cell cycle profile was detected by BD FACSCalibur Flow Cytometer (BD Biosciences) and analyzed by ModFit LT.

Transwell Assay

The lower chamber of a 24-well Transwell filter plate (Corning Incorporated, Corning, NY, USA) was filled with 800 µL of serum-containing medium supplemented with TGF-β_2. Each upper chamber was seeded with 2×10^4 LECs suspended in 100 µL of serum-free medium containing TGF-β_2. After 24 hours, cells attached to the upper side of the membrane were removed with a wet cotton swab. Transmigrated cells adhering to the underside of the membrane were fixed with 4% paraformaldehyde and subsequently stained with crystal violet (Beyotime). Three images of each Transwell plate were captured using an inverted microscope, and ImageJ (Media Cybernetics, Inc., Silver Spring, MD, USA) was used for quantification.

Scratch Wound Healing Assay

Scratches were made with a 200-µL pipette tip when cells reached 90% confluence in a 6-well plate. After removing detached cells with PBS, the remaining attached cells were cultured in serum-free DMEM with or without TGF-β_2 for 24 hours. We used a phase-contrast microscope to capture images of the wound area at both 0 and 24 hours. The wound area and the migration rate were calculated and analyzed using ImageJ software.

Statistical Analysis

Statistical analysis was conducted using GraphPad Prism version 8.2.1 (GraphPad Software, Inc., San Diego, CA, USA). Data from each group are expressed as mean ± SEM. A significance level of $P < 0.05$, determined using a two-tailed *t*-test or one-way ANOVA, was considered statistically significant.

Results

Smurf1 Exhibited Upregulation in Both Patients With ASC and Mice With Injury-Induced ASC

To evaluate the overall change of gene expression in fibrotic cataract, we conducted RNA-sequencing on lens capsules collected from an injury-induced ASC mouse model 7 days after surgery. Lens capsules from mice that underwent a sham operation, involving only corneal incision without lens capsule incision, served as the control group. The results of the GO enrichment analysis showed that the differentially expressed genes (DEGs) were enriched in the "response to wounding" term, which was in alignment with the process of injury-induced ASC. Additionally, we also observed enrichment in terms related to cell proliferation, cell migration, EMT, TGF-β/BMP, and Notch signaling pathways, consistent with the mechanism of ASC formation.[16,35,36] Moreover,

the GO analysis highlighted the involvement of the UPP, suggesting its potential role in ASC regulation (Fig. 1A). The heatmap of DEGs associated with cell proliferation (Fig. 1B), EMT (Fig. 1C), cell migration (Fig. 1D), and UPP (Fig. 1E) demonstrated an overall upregulation in these four processes in the ASC group compared to the control group. Considering the known importance of the TGF-β/BMP signaling pathway in ASC formation,[16] we aimed to identify any potential connection between the TGF-β/BMP signaling and the UPP in the regulation of ASC. Smurf1 functions as an E3 ubiquitin protein ligase that regulates TGF-β/BMP signaling pathway,[37] so we examined the mRNA and protein levels of Smurf1 in mouse ASC model and control group. The results of real-time PCR and Simple Western analysis revealed the upregulation of Smurf1 in the ASC group (Figs. 1F–H). Additionally, higher mRNA and protein levels of Smurf1 were observed in anterior capsules from the patients with ASC compared to the transparent lenses (Figs. 1I–K), suggesting a potential role for Smurf1 as a novel regulator of cataract formation.

Inhibition of Smurf1 Suppressed the Formation of Injury-Induced ASC in the Mouse

To investigate the impact of Smurf1 on fibrotic cataract progression, we used A01, a high-affinity selective Smurf1 inhibitor that blocks the interaction between the WW1 domain of Smurf1 and Smad1/5,[38] in a mouse model of injury-induced ASC. Whole-mount immunofluorescence of the anterior capsule, displaying the maximum cross-section and the vertical section, revealed that the A01 treatment group exhibited significantly smaller opacity compared to the control group (Fig. 2A). The 3D-reconstruction results of the subcapsular plaque, utilizing DAPI as a nuclear marker, indicated a significant reduction in opacity volume due to A01 treatment. Additionally, the volume of α-SMA, an EMT marker, was effectively suppressed by A01 treatment (Fig. 2B). Consistently, Simple Western analysis results demonstrated downregulation of the protein levels of EMT markers (fibronectin and N-cadherin), along with upregulation of the epithelial cell marker (E-cadherin), upon A01 treatment (Figs. 2C, 2D). These findings substantiate that in vivo inhibition of Smurf1 with A01 effectively attenuated both fibrotic cataract formation and the EMT of LECs.

Smurf1 Regulated the Proliferation of LECs

To validate the results in vivo, we established an in vitro cell culture model using the SRA01/04 cell line by manipulating the expression of Smurf1. As demonstrated in Supplementary Figure S2, the use of shRNA effectively reduced the protein level, whereas overexpression of an exogenous gene substantially increased its expression. The CCK-8 assay results indicated that knockdown of Smurf1 decreased the number of live LECs and overexpression of Smurf1 increased the number of live LECs (Figs. 3A, 3B). Simple Western analysis of the protein level of proliferating cell nuclear antigen (PCNA), which is a marker of proliferating cells,[39] revealed that Smurf1 knockdown decreased the protein level of PCNA, whereas Smurf1 overexpression increased PCNA protein level (see Figs. 3C–F). Moreover, the results of EdU incorporation consistently affirmed the regulatory role of Smurf1 in LEC proliferation (Figs. 3G–J). Consistently, results of the cell cycle profile analysis by flow cytometry showed that Smurf1 knockdown reduced the proportion of cells in S phase whereas Smurf1 overexpression increased the proportion of cells in S phase (Fig. 3K). The representative DNA fluorescence histograms of PI-stained LECs are shown in Supplementary Figure S3. In summary, Smurf1 knockdown restrained LEC proliferation, whereas Smurf1 overexpression facilitated LEC proliferation.

Smurf1 Regulated the Migration of LECs

Following the confirmation of Smurf1's role in LEC proliferation, we investigated its impact on LEC migration. It is well-established that TGF-β_2 promotes migration of LECs,[40] so we utilized TGF-β_2 to stimulate LEC migration. The results were presented by the crystal violet-stained cells that migrated and clung to the bottom membrane and the healing rates of the wound area (see Figs. 4A, 4B). The results from the Transwell assay and wound healing assay revealed that Smurf1 knockdown inhibited LEC migration in the presence or absence of TGF-β_2 (Figs. 4C, 4D). In contrast, overexpression of Smurf1 promoted the migration of LECs and also enhanced the TGF-β_2-induced migration of LECs (Figs. 4E, 4F). The results collectively revealed that Smurf1 knockdown inhibited LEC migration, whereas Smurf1 overexpression promoted LEC migration.

Smurf1 Regulated the EMT of LECs Induced by TGF-β_2

In the subsequent investigation, we explored the influence of Smurf1 on the EMT of LECs by using TGF-β_2 for 48 hours to induce EMT. The immunofluorescence results corroborated that TGF-β_2 upregulated the expression of the EMT marker fibronectin in both control and Smurf1 knockdown/overexpression cell lines. Smurf1 knockdown diminished the expression of fibronectin (Figs. 5A, 5B), whereas Smurf1 overexpression elevated fibronectin levels in the presence of TGF-β_2 (Figs. 5C, 5D). Moreover, as revealed by Simple Western analysis, when the LECs were treated with TGF-β_2, Smurf1 knockdown curtailed the TGF-β_2-induced increase in protein levels of fibronectin and N-cadherin, and ameliorated the TGF-β_2-induced reduction in ZO-1 protein level (Figs. 5E, 5F). Conversely, Smurf1 overexpression strengthened the impact of TGF-β_2 (Figs. 5G, 5H). However, knockdown or overexpression of Smurf1 alone showed no effect on the EMT of LECs in the absence of TGF-β_2. Taken together, Smurf1 knockdown restrained, whereas Smurf1 overexpression stimulated the EMT of LECs induced by TGF-β_2.

Smurf1 Regulated the Protein Level of Smad1, Smad5, and pSmad1/5

After confirming the impact of Smurf1 on ASC formation and LECs' biological behavior, we conducted further investigation into the underlying mechanism by transcriptome sequencing with LECs. The GO enrichment analysis of TGF-β_2-treated Smurf1 knockdown LECs and TGF-β_2-treated normal control LECs revealed that the DEGs were enriched to terms related to biological processes, such as cell migration, cell junction, and cell-matrix adhesion. In addition, DEGs exhibited enrichment in TGF-β/BMP signaling pathway and Smad protein phosphorylation (Fig. 6A). Simple Western analysis was conducted to

Investigative Ophthalmology & Visual Science

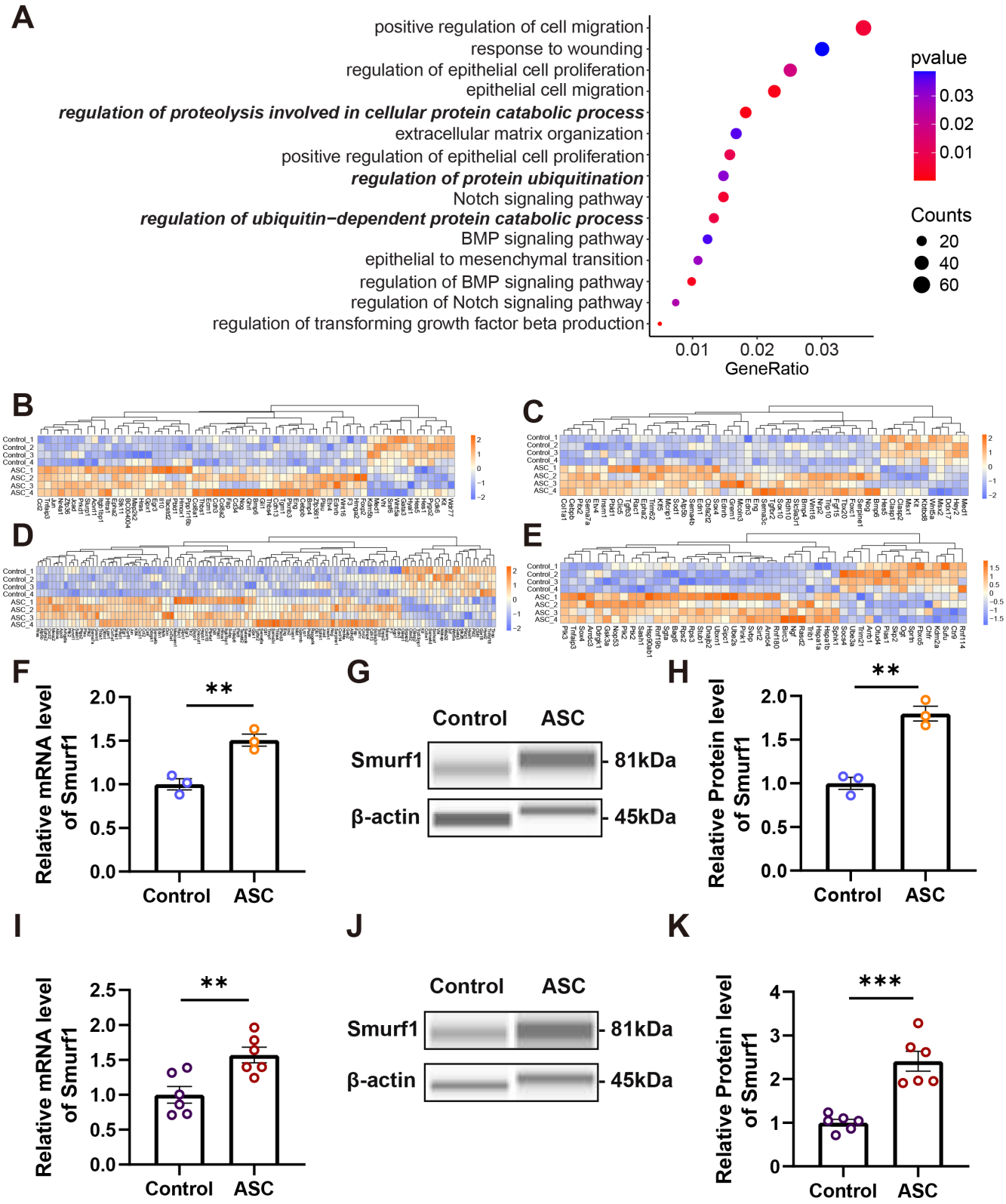

Figure 1. Smurf1 exhibited upregulation in both patients with ASC and mice with injury-induced ASC. (**A**) Dot plot of GO enrichment analysis comparing control croup and mouse ASC model group. Each dot represents a GO term, with its size indicating the number of genes in that particular GO term (count). The position along the X-axis (GeneRatio) signifies the ratio of the genes found enriched in the named pathway. The color (*P* value) represents the significance of enrichment. Terms related to ubiquitin-proteasome pathway were shown in bold italics. (**B**) Heatmap illustrating the expression profiles of DEGs associated with cell proliferation. The color gradient reflects the gene expression levels, with warmer colors (*orange*) indicating higher expression and cooler colors (*violet*) indicating lower expression. Each group has four biological replicates. (**C**) Heatmap of DEGs associated with EMT. (**D**) Heatmap of DEGs related to cell migration. (**E**) Heatmap of DEGs related to ubiquitin-proteasome pathway. (**F**) Relative mRNA expression of Smurf1 in control and ASC group in mouse. The relative

level of mRNA was calculated using the $2^{-\Delta\Delta CT}$ method. β-actin served as loading control. (**G, H**) Representative Simple Western analysis results and statistical analysis of relative Smurf1 protein expression in control and ASC group in mouse. β-actin was used as loading control. (**I**) Relative mRNA level of Smurf1 in anterior capsules of transparent human lenses (control) and patients with ASC. (**J, K**) Simple Western analysis results and statistical analysis of relative protein level of Smurf1 in anterior capsules of control and ASC group in humans. Data are displayed as mean ± SEM from three independent experiments. $^{**}P < 0.01$, $^{***}P < 0.001$.

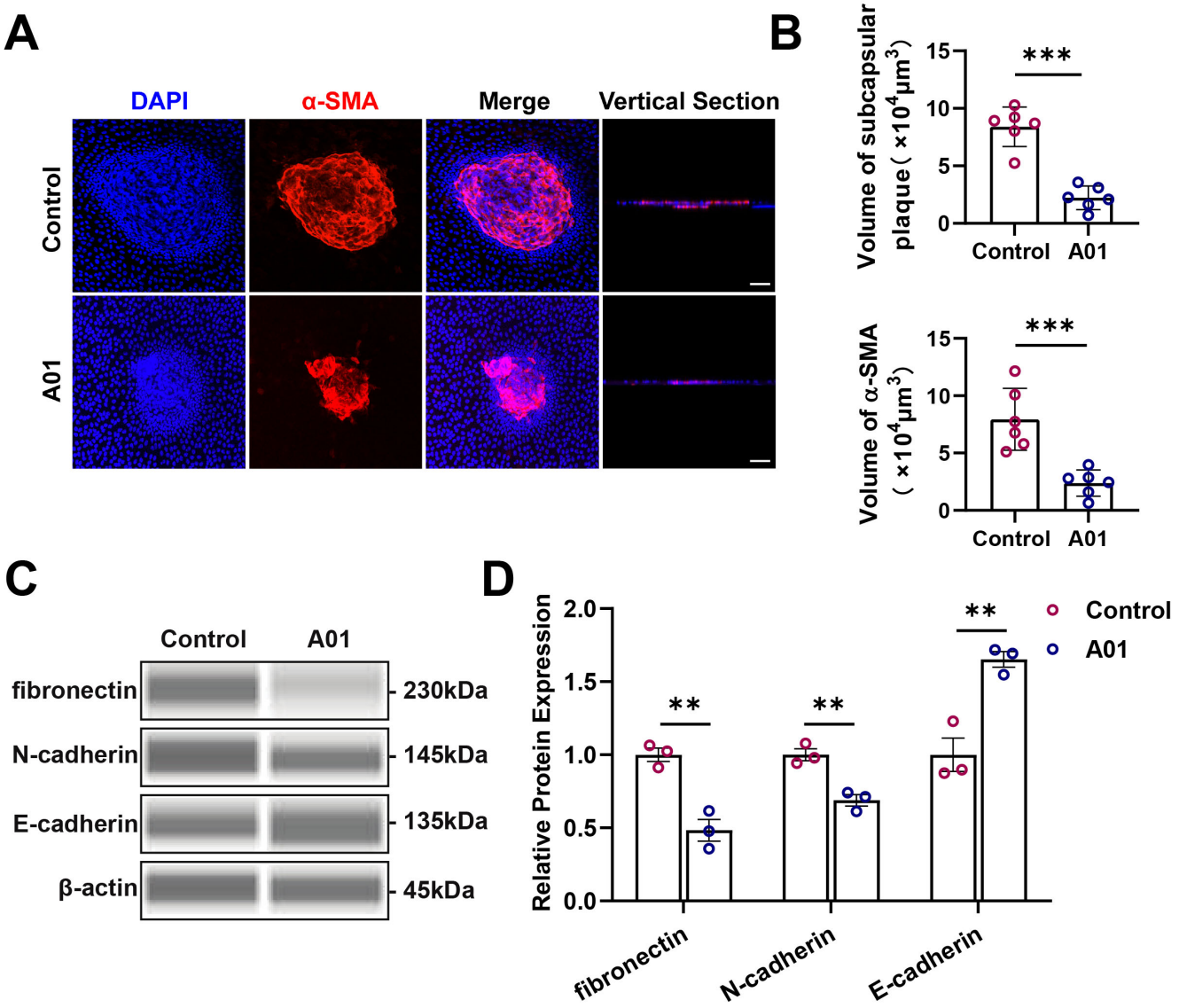

Figure 2. Inhibition of Smurf1 suppressed the formation of injury-induced ASC in mouse. (**A**) Representative immunofluorescence images of whole-mount anterior capsule. Horizontal images depict the section with the largest plaque area, whereas the vertical section illustrates plaque thickness. DAPI (*blue*) for the nuclei and α-SMA (*red*) for the EMT marker. Scale bar = 50 µm. (**B**) Quantification and statistical analysis of plaque volume (indicated by nuclei volume) and α-SMA volume. Six samples of anterior lens capsules were utilized for statistical analysis in each group. (**C**) The protein levels of fibronectin, N-cadherin, and E-cadherin were analyzed using Simple Western analysis, and the output electrophoretogram with HDR exposure was displayed. β-actin was used as the loading control. (**D**) Statistical analysis of relative protein levels normalized to β-actin. Data is shown as mean ± SEM from three independent experiments. $^{**}P < 0.01$, $^{***}P < 0.001$.

validate the results of RNA-seq. The results showed that Smurf1 knockdown elevated, whereas Smurf1 overexpression diminished the total protein levels of Smad1, Smad5, and the phosphorylation levels of Smad1/5 (pSmad1/5) in the presence or absence of TGF-β_2. However, neither Smurf1 knockdown nor overexpression affected the total protein level of Smad2, Smad3, or the phosphorylation levels of Smad2/3 (pSmad2/3). Additionally, TGF-β_2 treatment decreased Smad1/5 phosphorylation and increased Smad2/3 phosphorylation while showing no impact on the total levels of Smad1, Smad2, Smad3, or Smad5 (Figs. 6B–E). We then assessed the protein levels of Smads in both the A01-treated and the control group of mouse ASC model to verify the results we observed in vitro. The Simple West-

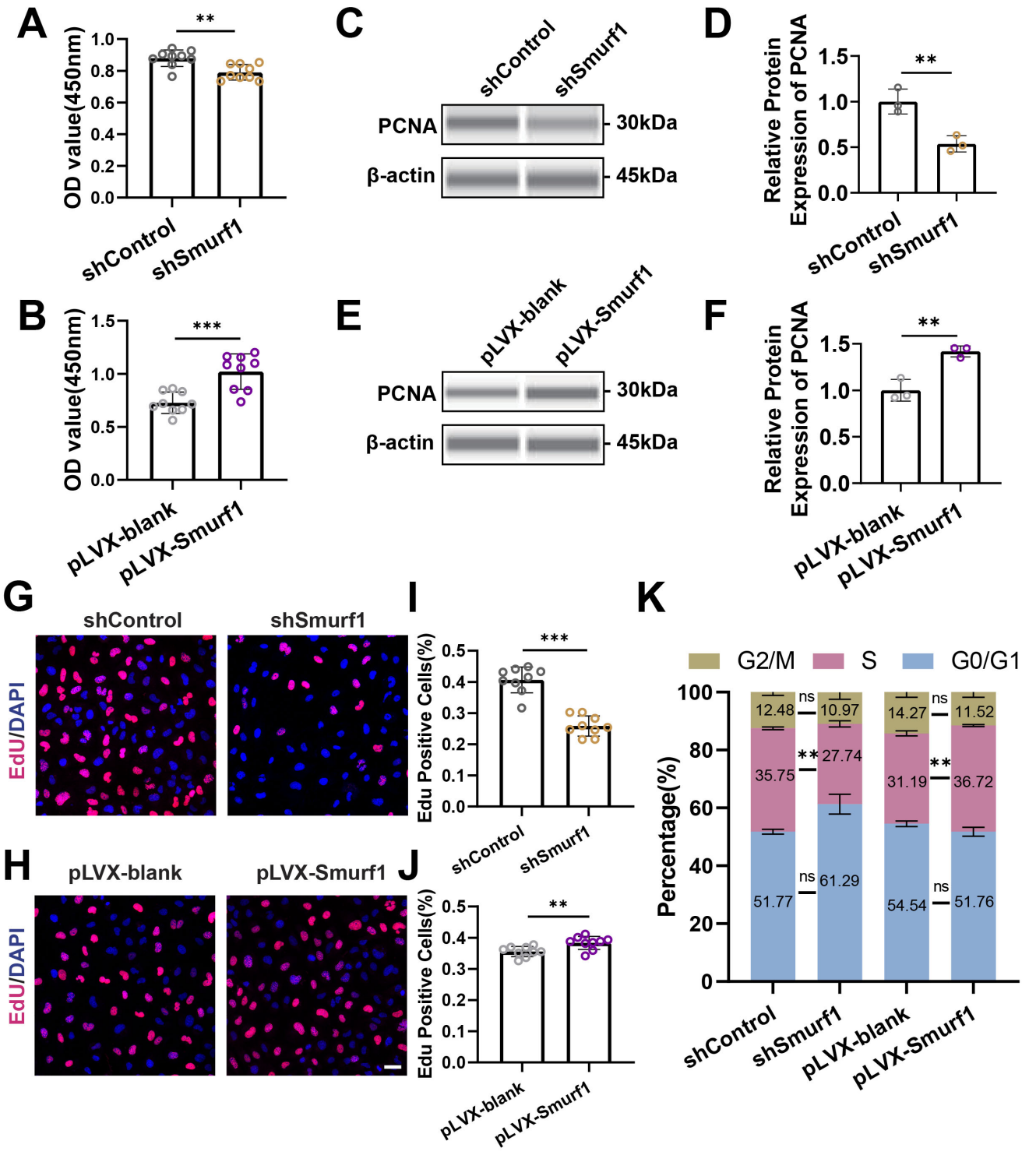

Figure 3. Smurf1 regulated the proliferation of LECs. (**A**) Absorbance readings at 450 nm from CCK-8 assays for Smurf1 knockdown and negative control groups. (**B**) Absorbance values at 450 nm from CCK-8 assays for Smurf1 overexpression and control groups. (**C, D**) Simple Western analysis results and statistical analysis of relative protein level of PCNA in Smurf1 knockdown cell line and negative control. (**E, F**) Relative PCNA protein level and its statistical analysis of Smurf1 overexpression cell line and negative control. (**G, H**) Immunofluorescence results of EdU incorporation in Smurf1 knockdown or overexpression cell line compared to negative control. Scale bar = 50 µm. (**I, J**) Quantification of the percentage of EdU-positive cells. (**K**) Results of the cell cycle analysis by flow cytometry showing the percentage of cells in G2/M, S, or G0/G1 phase of Smurf1 knockdown, Smurf1 overexpression, and respective control groups. Results are displayed as mean ± SEM from three independent experiments. $^{**}P < 0.01$, $^{***}P < 0.001$, ns, no statistical significance.

Investigative Ophthalmology & Visual Science

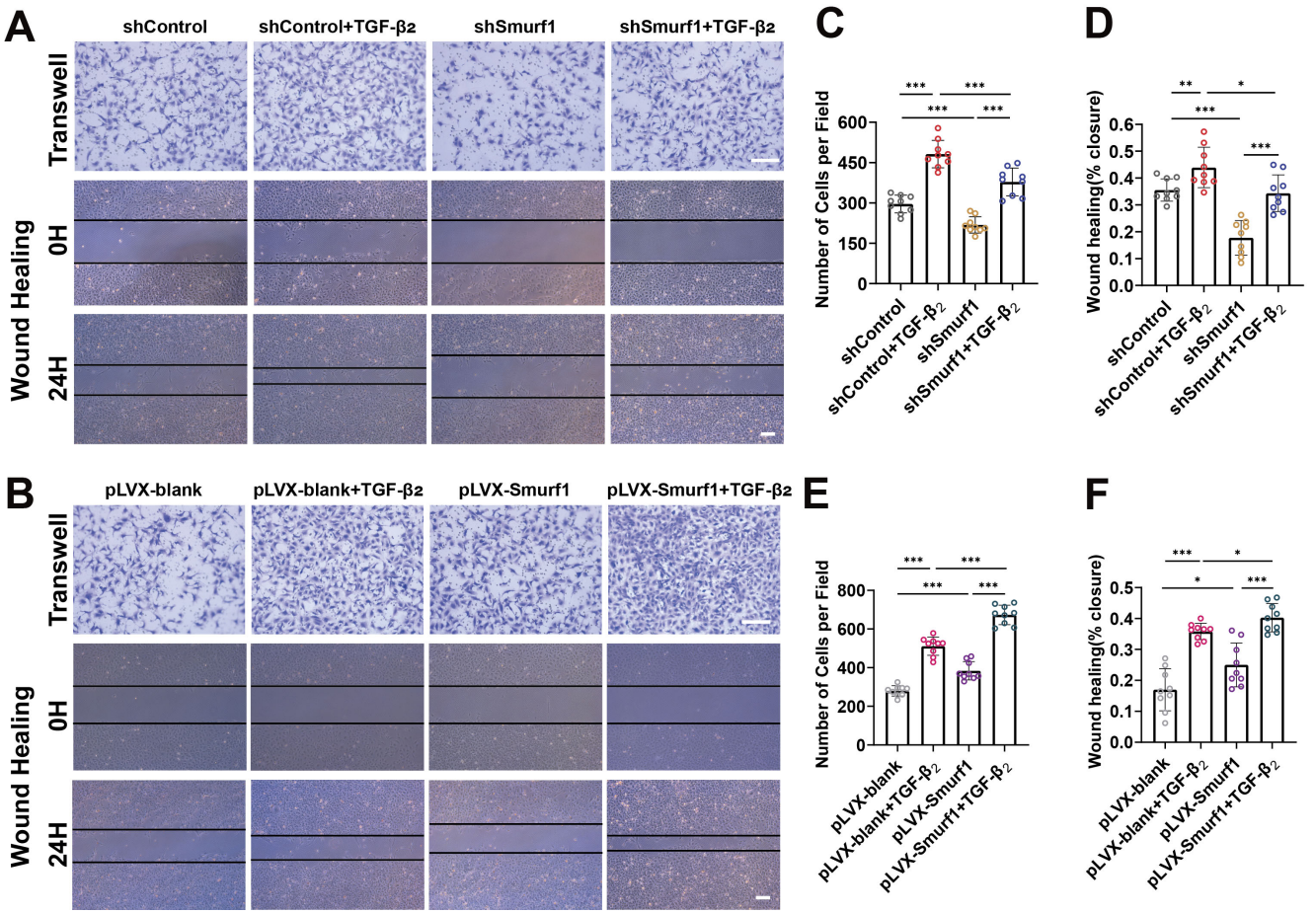

Figure 4. Smurf1 regulated the migration of LECs. (**A, B**) Representative images of cells that migrated through the porous membrane, stained with crystal violet, and time-lapse images depicting the closure of the cell-free gap over 24 hours shown by *straight black lines*. Images were captured using an inverted microscope. Scale bar = 200 µm. (**C, E**) Quantitative analysis of migrated cells presented as the average number of cells per field of view. (**D, F**) Quantification and statistical analysis of the wound closure rate represented as the percentage of the wound area at 24 hours compared to it at 0 hours. Data are expressed as mean ± SEM of nine images per group from three parallel experiments. $^{*}P < 0.05$, $^{**}P < 0.01$, $^{***}P < 0.001$.

ern analysis results revealed that A01 treatment upregulated the total protein levels of Smad1, Smad5, and the Smad1/5 phosphorylation, while exerting no impact on the total protein levels of Smad2, Smad3, or the Smad2/3 phosphorylation level (Figs. 6F, 6G), which was consistent with the results in vitro. In summary, Smurf1 regulates fibrotic cataract by modulating the protein levels of Smad1, Smad5, and pSmad1/5.

Discussion

In this study, we have identified Smurf1 as a pivotal link between the UPP and the TGF-β/BMP signaling pathway, playing a crucial role in the regulation of fibrotic cataract. We conducted RNA sequencing analysis and identified the upregulated expression of genes related to UPP. Notably, our investigation revealed elevated level of Smurf1 in a mouse ASC model. This increased expression of Smurf1 was further confirmed in lens capsules obtained from patients afflicted with ASC. Then, we demonstrated that inhibiting Smurf1 with A01 effectively curbed ASC formation by suppressing EMT. Additionally, our research delved into the functional significance of Smurf1 in LEC proliferation, migration, and EMT. We also establish that Smurf1's regulatory role is mediated through its modulation of Smad1, Smad5, and pSmad1/5, which are key components of the BMP signaling pathway.

The UPS is a highly precise system for protein degradation in eukaryotes.[41,42] To initiate ubiquitination, ubiquitin molecules are initially activated through the ubiquitin-activating enzyme (E1). Following activation, ubiquitin is transferred to ubiquitin-conjugating enzyme (E2), followed by the formation of a bond between the ubiquitin and the specific substrate protein, which requires substrate-specific ubiquitin ligase (E3). Ultimately, the ubiquitinated substrate undergoes degradation by proteasomes.[43–45] UPS is reported to be related to the formation of cataract. For instance, targeted expression of K6W mutant ubiquitin in mouse lens results in lens developmental abnormalities and the formation of cataract.[46] Moreover, altered ubiquitination of crystallins has been identified as a causative factor in their aggregation and precipitation, leading to lens opacification.[47,48] Additionally, the proteasome inhibitor MG132 inhibited the PCO progression in rabbit PCO model as well as suppressed the EMT marker in HLE B-3 cell line.[49,50] Our RNA sequencing data further underscored the involvement of the UPP in fibrotic cataract, as evidenced by its upregulation in the

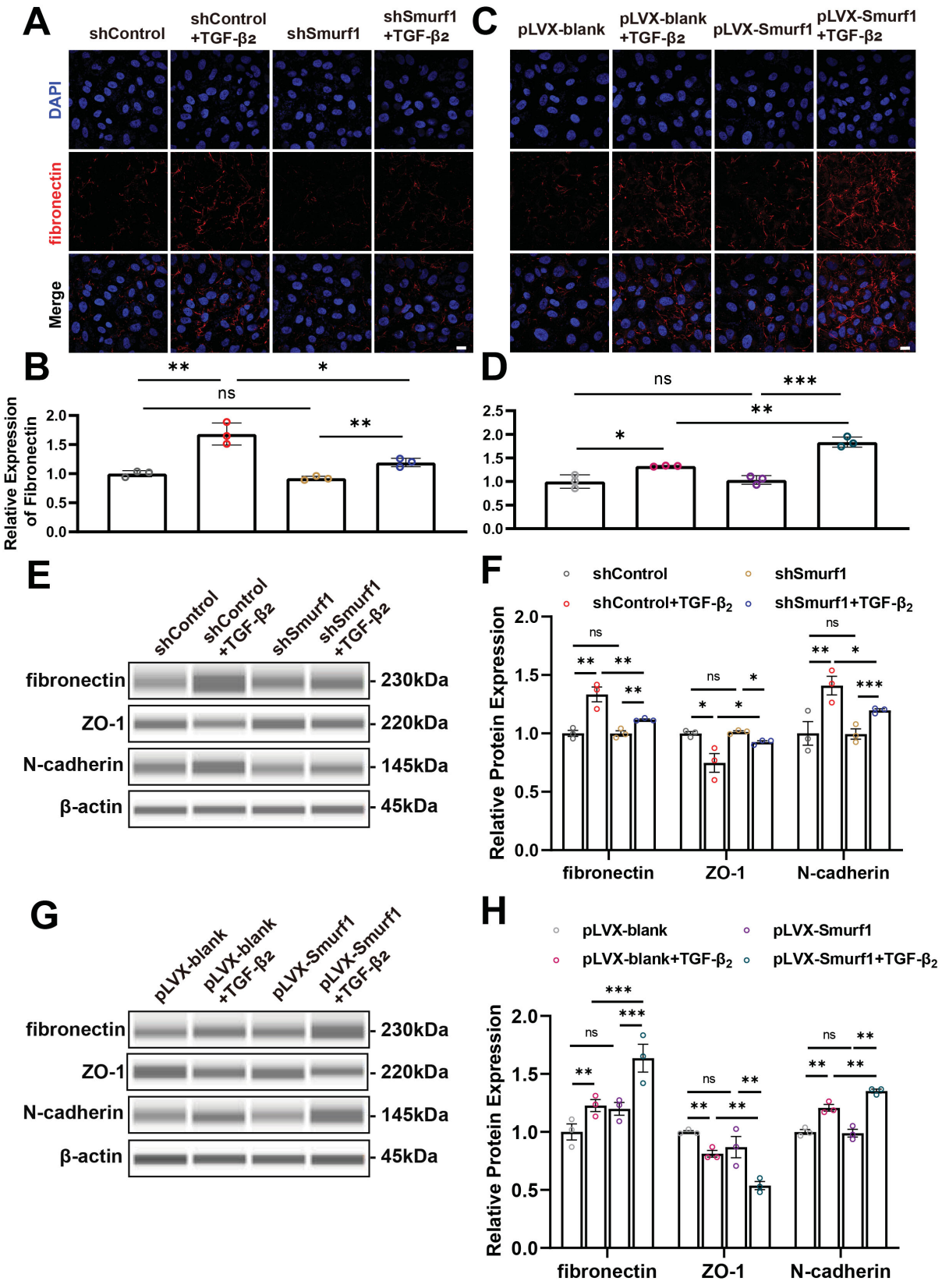

Figure 5. Smurf1 regulated the EMT of LECs induced by TGF-β_2. (**A, C**) Representative images illustrating fibronectin (*red*) distribution in cells of the Smurf1 knockdown or overexpression group and respective normal controls in the presence or absence of TGF-β_2 with nuclei counterstained with DAPI (*blue*). Scale bar = 25 µm. (**B, D**) Quantification and statistical analysis of relative fibronectin fluorescence intensity. (**E, G**) Representative Simple Western analysis bands illustrating the expression of fibronectin, ZO-1, and N-cadherin. β-actin served as loading control. (**F, H**) Statistical analysis of relative protein expression, presented as the relative fold change compared to the normal control group. Data is shown as mean ± SEM from three independent experiments. $^{*}P < 0.05$, $^{**}P < 0.01$, $^{***}P < 0.001$, ns, no statistical significance.

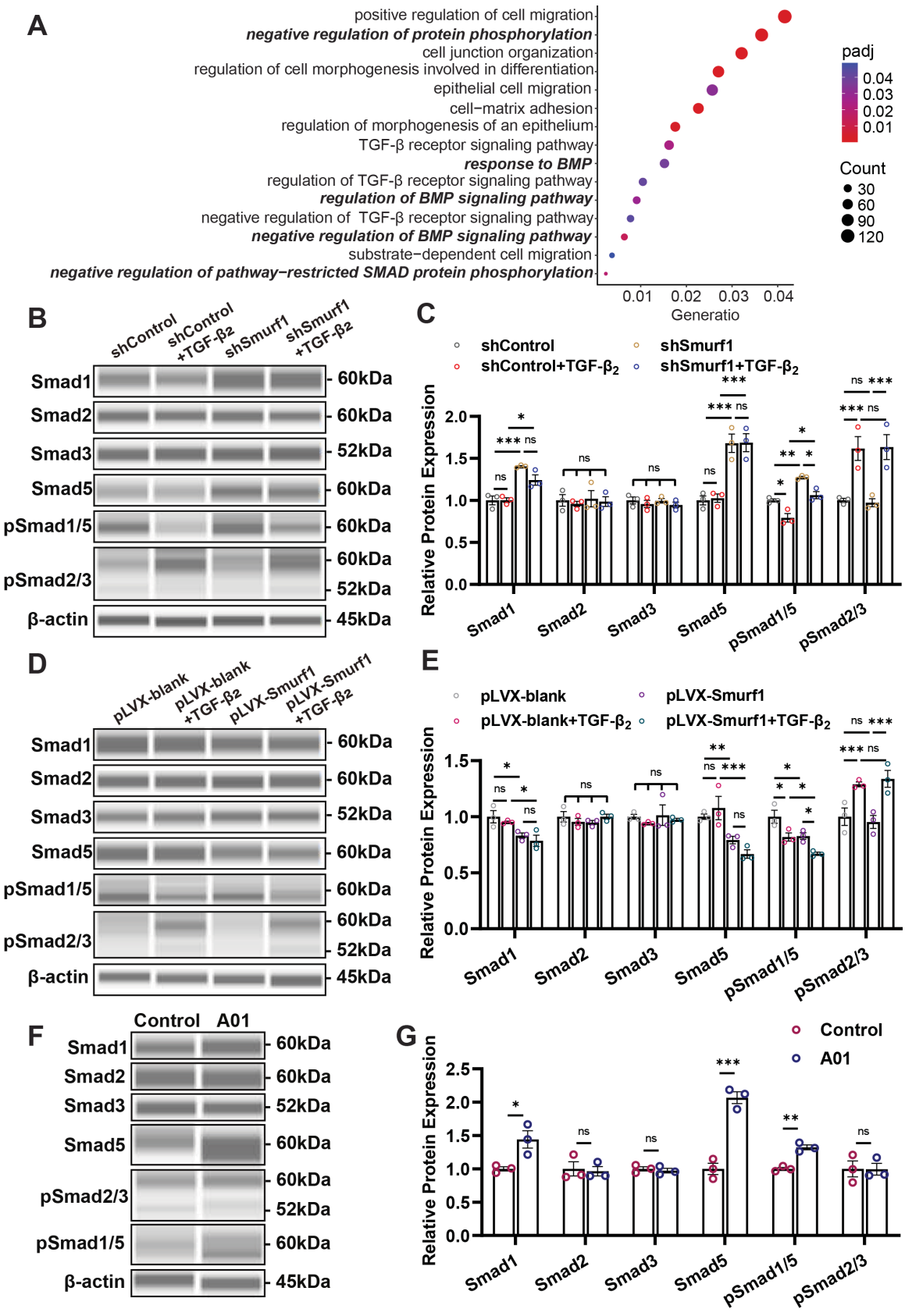

Figure 6. Smurf1 regulated the protein level of Smad1, Smad5 and pSmad1/5. (**A**) Dot plot illustrating the results of GO enrichment analysis. The size of each *dot* corresponds to the number of genes enriched in the respective GO term. The X-axis represents the Generatio, whereas the Y-axis indicates the specific GO terms. The *dots* are color-coded based on the significance of enrichment (padj value). Terms

related to BMP signaling pathway and Smad protein phosphorylation are shown in bold italic. (**B, C**) Simple Western analysis results and the statistical analysis showed the relative protein level of Smad1, Smad2, Smad3, Smad5, pSmad1/5, and pSmad2/3 normalized to β-actin in Smurf1 knockdown and negative control cell lines. (**D, E**) Images and statistical analysis of Simple Western analysis results displayed the relative protein levels in Smurf1 overexpression and negative control cell lines. (**F, G**) Images and quantification of Simple Western analysis results of lens capsules from control and A01-treated ASC model. Data are presented as the mean of relative fold change ± SEM from three independent experiments. $^{*}P < 0.05$, $^{**}P < 0.01$, $^{***}P < 0.001$, ns, no statistical significance.

mouse ASC model. To narrow down our focus within the UPP, we turned our attention to the substrate-specific ubiquitin ligase. Given its role as a regulator of the TGF-β/BMP signaling pathway,[41] Smurf1 emerged as a promising candidate. Indeed, our investigation revealed an upregulation of Smurf1 in patients with ASC and the mouse ASC model, strongly suggesting its regulatory significance in the context of fibrotic cataract.

Research on Smurf1 has predominantly centered around its involvement in cancer,[51] with its role in cataract formation receiving comparatively little attention. However, our current study highlights new findings in this regard. The application of A01 was demonstrated to effectively hinder the progression of ASC in a mouse model, concomitantly reducing the levels of EMT markers. Then, we established Smurf1 knockdown and overexpression cell lines and further elucidated that Smurf1 knockdown inhibited while Smurf1 overexpression facilitated the proliferation, migration, and EMT of LECs. These findings reveal the pivotal role of Smurf1 in cataract formation, shedding new light on its functional significance beyond its well-documented involvement in cancer research.

To further explore the mechanism underlying Smurf1-mediated ASC suppression, we conducted a transcriptome sequencing on LECs. The results suggested the involvement of TGF-β/BMP-Smad signaling pathway and the phosphorylation of Smads. The regulatory role of Smurf1 within the TGF-β/BMP signaling pathway is intricate. Whereas initial reports primarily emphasized its capacity to degrade Smad1 and Smad5,[25] subsequent research has unveiled its multifaceted interactions with various components of the TGF-β/BMP signaling pathway. Specifically, Smurf1 has been documented to induce the ubiquitination and cytoplasmic localization of Smad7.[52] Moreover, Smurf1 was found to induce the ubiquitination and degradation of TβRI,[53] BMPRI,[54] and Smad4[55] with assistance from Smad7 or R-Smads which functioned as the adaptor in this process. Meanwhile, in this study, we also showed that inhibition of Smurf1 led to upregulation in the protein levels of Smad1 and Smad5 and overexpression of Smurf1 resulted in their downregulation, aligning with previous findings. Notably, we also observed a similar pattern in the levels of pSmad1/5, indicative of their active state, upon Smurf1 inhibition and overexpression. Because Smad1 and Smad5 are downstream components of the BMP signaling pathway, these results indicate that the elevation of Smurf1 led to a decrease in BMP signaling. In consistency, the variation of Smurf1 had no significant effect on Smad2 or Smad3, which are components of the TGF-β signaling pathway. Thus, these results suggest that the impact of Smurf1 is probably exerted via regulating the inhibition of the BMP signal over the TGF-β pathway. Nevertheless, we cannot exclude the intricate interplay of Smurf1 with I-Smad (Smad6 and Smad7), Co-Smad (Smad4), and the receptors of the TGF-β/BMP, which requires further exploration in the future.

In conclusion, our data from clinical samples of human, mouse ASC model and human lens epithelial cell line collectively illuminate the involvement of Smurf1 in the development of fibrotic cataract through the modulation of the Smad signaling pathway. Our discoveries extend our understanding of fibrotic cataract and indicate the significance of Smurf1 in both its prevention and treatment.

Acknowledgments

Supported by grants from the National Natural Science Foundation of China (No. 81970783 and No. 81770909).

Disclosure: **F. Jiang**, None; **Y. Yang**, None; **Y. Ni**, None; **Y. Qin**, None; **F. Yuan**, None; **R. Ju**, None; **M. Wu**, None

References

1. Wormstone IM. Posterior capsule opacification: a cell biological perspective. *Exp Eye Res*. 2002;74:337–347.
2. GBD 2019 Blindness and Vision Impairment Collaborators; Vision Loss Expert Group of the Global Burden of Disease Study. Causes of blindness and vision impairment in 2020 and trends over 30 years, and prevalence of avoidable blindness in relation to VISION 2020: the Right to Sight: an analysis for the Global Burden of Disease Study. *Lancet Glob Health*. 2021;9:e144–e160.
3. Moisseiev J, Bartov E, Schochat A, Blumenthal M. Long-term study of the prevalence of capsular opacification following extracapsular cataract extraction. *J Cataract Refract Surg*. 1989;15:531–533.
4. Wei Z, Gordon P, Hao C, et al. Aged lens epithelial cells suppress proliferation and epithelial-mesenchymal transition-relevance for posterior capsule opacification. *Cells*. 2022;11:2001.
5. Jing R, Hu C, Qi T, et al. FILIP1L-mediated cell apoptosis, epithelial-mesenchymal transition and extracellular matrix synthesis aggravate posterior capsular opacification. *Life Sci*. 2021;286:120061.
6. Alfonso JF, Lisa C, Abdelhamid A, Fernandes P, Jorge J, Montés-Micó R. Three-year follow-up of subjective vault following myopic implantable collamer lens implantation. *Graefes Arch Clin Exp Ophthalmol*. 2010;248:1827–1835.
7. Nakamura T, Isogai N, Kojima T, Yoshida Y, Sugiyama Y. Posterior chamber phakic intraocular lens implantation for the correction of myopia and myopic astigmatism: a retrospective 10-year follow-up study. *Am J Ophthalmol*. 2019;206:1–10.
8. Imaizumi T, Kurosaka D, Tanaka U, Sakai D, Fukuda K, Sanbe A. Topical administration of a ROCK inhibitor prevents anterior subcapsular cataract induced by UV-B irradiation. *Exp Eye Res*. 2019;181:145–149.
9. Dilley KJ, Bron AJ, Habgood JO. Anterior polar and posterior subcapsular cataract in a patient with retinitis pigmentosa: a light-microscopic and ultrastructural study. *Exp Eye Res*. 1976;22:155–167.
10. Shirai K, Okada Y, Saika S. Immunohistochemical observation of anterior subcapsular cataract in eye with spontaneously regressed retinoblastoma. *J Cataract Refract Surg*. 2010;36:503–507.

11. Shu DY, Ong K, Lovicu FJ. Histopathology of subcapsular cataract in a patient with atopic dermatitis. *Optom Vis Sci*. 2017;94:270–276.
12. Petrash CC, Palestine AG, Smith J, Davidson R, Pantcheva MB. Iris retraction without hypotony. *Ophthalmol Ther*. 2022;11:1273–1279.
13. Wang X, Wang L, Sun Y, et al. MiR-22-3p inhibits fibrotic cataract through inactivation of HDAC6 and increase of α-tubulin acetylation. *Cell Prolif*. 2020;53:e12911.
14. Ishida I, Saika S, Okada Y, Ohnishi Y. Growth factor deposition in anterior subcapsular cataract. *J Cataract Refract Surg*. 2005;31:1219–1225.
15. Ma B, Jing R, Liu J, Qi T, Pei C. Gremlin is a potential target for posterior capsular opacification. *Cell Cycle*. 2019;18:1714–1726.
16. Jiang F, Qin Y, Yang Y, et al. BMP-4 and BMP-7 inhibit EMT in a model of anterior subcapsular cataract in part by regulating the notch signaling pathway. *Invest Ophthalmol Vis Sci*. 2023;64:12.
17. Lovicu FJ, Schulz MW, Hales AM, et al. TGFbeta induces morphological and molecular changes similar to human anterior subcapsular cataract. *Br J Ophthalmol*. 2002;86:220–226.
18. de Iongh RU, Wederell E, Lovicu FJ, McAvoy JW. Transforming growth factor-beta-induced epithelial-mesenchymal transition in the lens: a model for cataract formation. *Cells Tissues Organs*. 2005;179:43–55.
19. Salazar VS, Gamer LW, Rosen V. BMP signalling in skeletal development, disease and repair. *Nat Rev Endocrinol*. 2016;12:203–221.
20. Hachana S, Larrivée B. TGF-β superfamily signaling in the eye: implications for ocular pathologies. *Cells*. 2022;11:2336.
21. Derynck R, Zhang YE. Smad-dependent and Smad-independent pathways in TGF-beta family signalling. *Nature*. 2003;425:577–584.
22. Macias MJ, Martin-Malpartida P, Massagué J. Structural determinants of Smad function in TGF-β signaling. *Trends Biochem Sci*. 2015;40:296–308.
23. Meng XM, Nikolic-Paterson DJ, Lan HY. TGF-β: the master regulator of fibrosis. *Nat Rev Nephrol*. 2016;12:325–338.
24. Liu J, Jin J, Liang T, Feng XH. To Ub or not to Ub: a regulatory question in TGF-β signaling. *Trends Biochem Sci*. 2022;47:1059–1072.
25. Zhu H, Kavsak P, Abdollah S, Wrana JL, Thomsen GH. A SMAD ubiquitin ligase targets the BMP pathway and affects embryonic pattern formation. *Nature*. 1999;400:687–693.
26. Tang LY, Yamashita M, Coussens NP, et al. Ablation of Smurf2 reveals an inhibition in TGF-β signalling through multiple mono-ubiquitination of Smad3. *Embo J*. 2011;30:4777–4789.
27. Xu Z, Greenblatt MB, Yan G, et al. SMURF2 regulates bone homeostasis by disrupting SMAD3 interaction with vitamin D receptor in osteoblasts. *Nat Commun*. 2017;8:14570.
28. Lin X, Liang M, Feng XH. Smurf2 is a ubiquitin E3 ligase mediating proteasome-dependent degradation of Smad2 in transforming growth factor-beta signaling. *J Biol Chem*. 2000;275:36818–36822.
29. Tao Y, Sun C, Zhang T, Song Y. SMURF1 promotes the proliferation, migration and invasion of gastric cancer cells. *Oncol Rep*. 2017;38:1806–1814.
30. Kwei KA, Shain AH, Bair R, et al. SMURF1 amplification promotes invasiveness in pancreatic cancer. *PLoS One*. 2011;6:e23924.
31. Gang X, Wang G, Huang H. Androgens regulate SMAD ubiquitination regulatory factor-1 expression and prostate cancer cell invasion. *Prostate*. 2015;75:561–572.
32. Xia Q, Li W, Ali S, et al. Smurf1 silencing restores PTEN expression that ameliorates progression of human glioblastoma and sensitizes tumor cells to mTORC1/C2 inhibitor Torin1. *iScience*. 2021;24:103528.
33. Li D, Wei TT, Cai J, Xie TH, Yao Y, Zhu L. Smurf1: a possible therapeutic target in dry age-related macular degeneration. *Exp Eye Res*. 2023;233:109549.
34. Xiao W, Chen X, Li W, et al. Quantitative analysis of injury-induced anterior subcapsular cataract in the mouse: a model of lens epithelial cells proliferation and epithelial-mesenchymal transition. *Sci Rep*. 2015;5:8362.
35. Lovicu FJ, Steven P, Saika S, McAvoy JW. Aberrant lens fiber differentiation in anterior subcapsular cataract formation: a process dependent on reduced levels of Pax6. *Invest Ophthalmol Vis Sci*. 2004;45:1946–1953.
36. Shu DY, Wojciechowski MC, Lovicu FJ. Bone Morphogenetic protein-7 suppresses TGFβ2-induced epithelial-mesenchymal transition in the lens: implications for cataract prevention. *Invest Ophthalmol Vis Sci*. 2017;58:781–796.
37. Brazil DP, Church RH, Surae S, Godson C, Martin F. BMP signalling: agony and antagony in the family. *Trends Cell Biol*. 2015;25:249–264.
38. Cao Y, Wang C, Zhang X, et al. Selective small molecule compounds increase BMP-2 responsiveness by inhibiting Smurf1-mediated Smad1/5 degradation. *Sci Rep*. 2014;4:4965.
39. Kurki P, Vanderlaan M, Dolbeare F, Gray J, Tan EM. Expression of proliferating cell nuclear antigen (PCNA)/cyclin during the cell cycle. *Exp Cell Res*. 1986;166:209–219.
40. Yang Y, Ye Y, Lin X, Wu K, Yu M. Inhibition of pirfenidone on TGF-beta2 induced proliferation, migration and epithelial-mesenchymal transition of human lens epithelial cells line SRA01/04. *PLoS One*. 2013;8:e56837.
41. Izzi L, Attisano L. Regulation of the TGFbeta signalling pathway by ubiquitin-mediated degradation. *Oncogene*. 2004;23:2071–2078.
42. Glickman MH, Ciechanover A. The ubiquitin-proteasome proteolytic pathway: destruction for the sake of construction. *Physiol Rev*. 2002;82:373–428.
43. Pohl C, Dikic I. Cellular quality control by the ubiquitin-proteasome system and autophagy. *Science*. 2019;366:818–822.
44. Liu W, Tang X, Qi X, et al. The ubiquitin conjugating enzyme: an important ubiquitin transfer platform in ubiquitin-proteasome system. *Int J Mol Sci*. 2020;21:2894.
45. Collins GA, Goldberg AL. The logic of the 26S proteasome. *Cell*. 2017;169:792–806.
46. Shang F, Wilmarth PA, Chang ML, et al. Newborn mouse lens proteome and its alteration by lysine 6 mutant ubiquitin. *J Proteome Res*. 2014;13:1177–1189.
47. Liu K, Lyu L, Chin D, et al. Altered ubiquitin causes perturbed calcium homeostasis, hyperactivation of calpain, dysregulated differentiation, and cataract. *Proc Natl Acad Sci U S A*. 2015;112:1071–1076.
48. Dudek EJ, Lampi KJ, Lampi JA, et al. Ubiquitin proteasome pathway-mediated degradation of proteins: effects due to site-specific substrate deamidation. *Invest Ophthalmol Vis Sci*. 2010;51:4164–4173.
49. Bao X, Hou M, Qin Y, Luo F, Shang F, Wu M. Effect of an MG132-sustained drug delivery capsular ring on the inhibition of posterior capsule opacification in a rabbit model. *J Ocul Pharmacol Ther*. 2017;33:103–110.
50. Hosler MR, Wang-Su ST, Wagner BJ. Role of the proteasome in TGF-beta signaling in lens epithelial cells. *Invest Ophthalmol Vis Sci*. 2006;47:2045–2052.
51. Fu L, Cui CP, Zhang X, Zhang L. The functions and regulation of Smurfs in cancers. *Semin Cancer Biol*. 2020;67:102–116.

Investigative Ophthalmology & Visual Science

52. Suzuki C, Murakami G, Fukuchi M, et al. Smurf1 regulates the inhibitory activity of Smad7 by targeting Smad7 to the plasma membrane. *J Biol Chem*. 2002;277:39919–39925.
53. Ebisawa T, Fukuchi M, Murakami G, et al. Smurf1 interacts with transforming growth factor-beta type I receptor through Smad7 and induces receptor degradation. *J Biol Chem*. 2001;276:12477–12480.
54. Murakami G, Watabe T, Takaoka K, Miyazono K, Imamura T. Cooperative inhibition of bone morphogenetic protein signaling by Smurf1 and inhibitory Smads. *Mol Biol Cell*. 2003;14:2809–2817.
55. Morén A, Imamura T, Miyazono K, Heldin CH, Moustakas A. Degradation of the tumor suppressor Smad4 by WW and HECT domain ubiquitin ligases. *J Biol Chem*. 2005;280:22115–22123.

Investigative Ophthalmology & Visual Science